Semiconductor Physics, Quantum Electronics & Optoelectronics, 2024. V. 27, No 2. P. 224-234.

Optoelectronics and optoelectronic devices

Modeling and simulation of a high power InGaP/GaAs heterojunction alphavoltaic battery irradiated by americium-241

F. Bouzid[1,*], E. Kayahan[2], M.A. Saeed[3], B. Babes[1], S.S.M. Ghoneim[4], F. Pezzimenti[5]

[1]*Research Center in Industrial Technologies CRTI, P.O. Box 64, Cheraga 16014, Algiers, Algeria*
[2]*Laser Technologies Research and Application Center (LATARUM), Kocaeli University, 41275, Yeniköy, Kocaeli, Turkey*
[3]*Department of Physics, Division of Science & Technology, University of Education, Lahore, Pakistan*
[4]*Electrical Engineering Department, College of Engineering, Taif University, P. O. Box 11099, Taif 21944, Saudi Arabia*
[5]*DIIES – Mediterranea University of Reggio Calabria, 89122 Reggio Calabria, Italy*
[*]*Corresponding author email: f.bouzid@crti.dz*

Abstract. The design of semiconductor-based heterojunction structures can be turned useful to raise the efficiency of nuclear micro-batteries. In this study, we have investigated a micro-power alphavoltaic battery by using a lab-made software. The nuclear battery consists of an $In_{0.49}Ga_{0.51}P$/GaAs heterostructure irradiated by americium-241 (Am^{241}) alpha particles with an average kinetic energy of 5.485 MeV. The alphavoltaic battery exhibits an overall active area of 1 cm^2. Based on a comprehensive analytical model, the device current density-voltage $J(V)$ and output electric power $P(V)$ characteristics are simulated extracting the energy conversion efficiency. The model takes into account the reflection of the incident alpha particles, the ohmic losses, the effect of the boundary between the two layers, and the depletion region borders. Different values of the radioisotope apparent activity density, the emitter and base dopant concentrations, and the surface recombination velocities in both the front and back layers are considered during the simulations to optimize the battery performance. The present study reports that by irradiating by a 2.4 mCi/cm^2 Am^{241} source, the obtained energy conversion efficiency of the battery can reach 10.31% with a maximum output power density of 16.07 $\mu W/cm^2$. Therefore, $In_{0.49}Ga_{0.51}P$/GaAs heterostructure coupled with Am^{241} seems a promising design for long-term energy supply in harsh environments.

Keywords: alphavoltaic battery, heterostructure, americium-241, alpha particles, ohmic losses.

https://doi.org/10.15407/spqeo27.02.224
PACS 73.40.Kp, 84.60.Bk, 85.30.De

Manuscript received 06.11.23; revised version received 22.03.24; accepted for publication 19.06.24; published online 21.06.24.

1. Introduction

As human interest in alternative, efficient and sustainable energy sources increases day by day, different natural resources are restlessly exploited and probed including energy emitted from radioactive materials. In the past, low-bandgap semiconductors were used to absorb photons from different types of hot radioactive sources. Such converters were applied *e.g.* to provide power for navigation and communication in many successful space missions since the 1960s. Moreover, by using semiconductor technology, other converters were designed to convert kinetic energy of alpha or beta particles emitted from radioactive materials into electrical energy, according to a mechanism that recalls photoelectric phenomena. In this context, alphavoltaic and betavoltaic nuclear batteries were considered for many applications and systems with low energy consumption. In particular, pacemakers powered by nuclear batteries were designed and implanted in thousands of patients. However, although the betavoltaic and alphavoltaic mechanisms were discovered long ago (Mosely, 1913) [1], and the first betavoltaic battery was reported in 1953 by Rappaport *et al.* [2], designing and manufacturing nuclear batteries did not see as much progress as did the photovoltaic field started to develop in the same period. The main reason for this is the low energy conversion efficiency, despite it is theoretically possible to raise

© V. Lashkaryov Institute of Semiconductor Physics of the NAS of Ukraine, 2024
© Publisher PH "Akademperiodyka" of the NAS of Ukraine, 2024

the energy density of nuclear batteries above the one of the chemical counterparts. Moreover, nuclear batteries are costly and require appropriate radioactive sources as well as expertise to deal with them. Furthermore, the common non-positive perception of nuclear energy by the general public should be taken into account. Therefore, marketing nuclear batteries is still undoubtedly a challenge.

During the past few decades, great efforts have been done to create effective nuclear batteries. Different natural and synthetic radioactive sources, such as H^3, Ni^{63}, Pm^{147}, Cs^{137}, Co^{60}, and Sr^{90} for beta radiation and Am^{241}, Po^{210}, Pu^{238} and Th^{228} for alpha radiation, have been tested. At the same time, different semiconductors, such as Si [3], GaN [4, 5], SiC [6, 7], diamond [8, 9], B_4C [10], SeS [10], AlGaAs [11], GaAs [12] and InGaP [13–15], have been also considered for the mentioned batteries. Alphavoltaic batteries have shown particular importance for various civil and military applications. The energy density reserves of the radioactive nuclei that emit alpha particles exceed those of the best chemical sources by many folds, and this may be a great service to humanity. However, alphavoltaic batteries still face an important technological issue that leads to rapid deterioration of electrical energy production. This issue consists in the damage by alpha rays to the semiconductor crystal structure coupled to a radioactive source. To reduce this damage, the research efforts are focused on unconventional battery designs comprising semiconductors suitable to withstand the impact of highly energetic alpha particles. In particular, the device structures should detect and convert the energy of alpha particles and heavy ions. Therefore, wide bandgap materials with a high damage threshold energy and high carrier mobility should be used. These theoretical bases prompted the researchers' interest for several semiconductor compounds. The most significant results obtained over the past two decades are summarized in Table 1.

Table 1. Literature data about different alphavoltaic batteries.

Material	Structure	Radio-isotope	Activity (mCi/cm^2)	Efficiency (%)	Ref.
Diamond	Schottky	Pu^{238}	2.1	3.6	[8]
Diamond	Schottky	Am^{241}	0.00885	0.83	[9]
SiC	*p-i-n*	Am^{241}	–	10	[10]
SiC	Schottky	Am^{241}	0.018	0.1	[16]
GaN	*p-i-n*	Am^{241}	–	10	[10]
B_4C	*p-i-n*	Am^{241}	–	10	[10]
SeS	*p-i-n*	Am^{241}	–	10	[10]
InGaP	*p-n*	Am^{241}	0.00056	0.04	[13]
InGaP	*p-n*	Po^{210}	0.141	3.2	[13]
InGaP	*n-i-p-i*	Po^{210}	0.14	4.1	[14]
InGaP	*n-i-p-i*	Po^{210}	280	10.4	[14]

Different designs, including *p-n*, *p-i-n*, *n-i-p-i*, and Schottky junctions, have been proposed, and different radioactive sources have been tested. The obtained maximum conversion efficiency was 10.4% for an InGaP battery (*n-i-p-i* structure) irradiated by a Po^{210} source with a radioactivity density of 280 mCi/cm^2 [14].

However, limited attempts to investigate the performance of heterojunction-based batteries, which could take benefit of the advantages of different materials in the device structure, have been inferred from the analysis of the literature sources. Heterojunction structures have been already known to improve conversion efficiency of different photovoltaic devices [17, 18].

In this work, we investigate the performance of an alphavoltaic heterojunction battery using a lab-made software and accurate analytical modeling. The battery consists of an *n*-type $In_{1-x}Ga_xP$ layer with $x = 0.51$ grown on a *p*-type GaAs substrate. It converts alpha radiation with an average decay energy of 5.485 MeV emitted by an Am^{241} source [1, 10]. Am^{241} radioisotope is a low-cost material and has a long half-life exceeding 400 years. Previous results on Am^{241}-based alphavoltaic batteries evidence this radioisotope as very attractive from a power density perspective [19]. The bandgap of InGaP and GaAs alloys are 1.9 and 1.42 eV, respectively. These materials have been reported to tolerate high doses of alpha particles [20]. The values of the InGaP threshold displacement energy (E_{th}) to generating defects for In, Ga, and P are 290, 255, and 115 keV, respectively [21]. At the same time, E_{th} values for Ga and As in GaAs are 255 and 270 keV, respectively [21]. Therefore, a long term stability and reliability of the designed device structure for harsh radiation environment applications may be expected.

To shed light on the performance of the proposed battery structure, we have used our simulation software which enables the analysis of current density-voltage $J(V)$ and power density-voltage $P(V)$ device characteristics. From the calculations, we have extracted the key alphavoltaic parameters of the battery, which are directly related to the physical properties of the materials and enable design optimization. Finally, the effects of increasing operation temperature on the output performance of the device have been evaluated in the 300…350 K temperature range.

2. Device structure

The schematic cross-section of the proposed $In_{0.49}Ga_{0.51}P$/GaAs alphavoltaic battery is shown in Fig. 1 (plot not to scale). An Am^{241} source emitting alpha particles is attached to the battery. The simulated device active area is 1 cm^2. As demonstrated experimentally in Ref. [22] and the references therein, an $In_{1-x}Ga_xP$ alloy with a Ga composition ratio of 0.51 ($In_{0.49}Ga_{0.51}P$) can be grown on a GaAs layer with appropriate lattice match. More specifically, the lattice mismatch rate Δ is given by [23]:

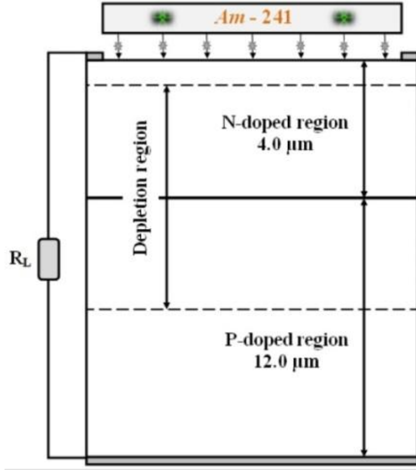

Fig. 1. Cross-sectional view of the $In_{0.49}Ga_{0.51}P/GaAs$ alphavoltaic battery.

$$\Delta = \frac{2\times(a_2 - a_1)}{(a_1 + a_2)},\qquad (1)$$

where a_1 and a_2 – lattice constants of GaAs and InGaP, respectively. Knowing that a_1(GaAs) = 5.65325 Å [24] and a_2(InGaP) = 5.655418 Å [25] the following empirical formula is applied for any value of x [25]:

$$a_2\left(\mathrm{In}_{1-x}\mathrm{Ga}_x\mathrm{P}_1\right) = 5.8687 - 0.4182x\,.\qquad (2)$$

For $x = 0.51$, the lattice mismatch rate is $\Delta = 0.038\%$. This value is an indication of a high quality $In_{0.49}Ga_{0.51}P/GaAs$ heterojunction.

The total thickness of the device is 16 μm, where the emitter thickness is 4 μm, the base thickness is 12 μm, and the depletion edge is located at the depth of 0.2 μm. These thicknesses are adopted for calculating the effective minority carrier diffusion lengths ($L_{h,e}$). In particular, the following values have been obtained: L_h = 1.7 μm in the InGaP layer and L_e = 16.26 μm in the GaAs layer.

As is well known, alpha particles have energies ranging from 4 to 10 MeV. Their path length spans from 5 to 10 μm in air and from 25 to 80 μm in a solid matter making this type of radiation the least penetrating [20]. Moreover, Am^{241} source appears very suitable to use in nuclear batteries because of its distinct properties such as significant decay energy, very long half-life, and absence of other types of more penetrating radiation. A comparison between alternative alpha particles sources is reported in Table 2.

The energy of the incoming alpha particles is transferred to the heterojunction by elastic and inelastic collisions. In more detail, Coulomb scattering induces production of several electron-hole pairs, the electrons and holes of which are separated in the depletion region (DR) and adjacent regions by the internal electric field. These carriers are drained to the external circuit through the battery electrodes. Free carriers formed far from the DR can also drift into the device structure contributing to the output current, although they rather tend to be involved in recombination processes.

Table 2. Comparison between alternative alpha-particles sources.

Isotope	Half-life (years)	E_{decay} (MeV)	$E_{average}$ (MeV)	Ref.
Am^{241}	432.2	5.638	5.485	[1, 10]
Pu^{238}	87.74	5.593	5.499	[1, 10]
Th^{228}	1.91	5.52	5.423	[1]
Po^{210}	0.379	5.305	5.304	[1, 27]

3. Modeling setup

3.1. Equivalent circuit

To study different operation conditions of the proposed $In_{0.49}Ga_{0.51}P/GaAs$ alphavoltaic battery, an equivalent circuit model, which includes one diode, was used. The diode comprises a series resistance R_s = 4.0 Ohm·cm^2 and a shunt resistance $R_{sh} = 6\cdot10^6$ Ohm cm^2. The R_{sh} value was fixed according to the approximate criterion [28]:

$$R_{sh} > 10\frac{V_{oc}}{I_{sc}},\qquad (3)$$

where V_{oc} and J_{sc} are the open-circuit voltage and the short-circuit current of the battery, respectively.

The ideality factor of the diode (quality factor), which is a measure of how closely the diode behavior follows the ideal model, was fixed to be 1.55. This dimensionless number characterizes deviations of the diode I–V curve from the ideal one due to recombination phenomena and/or high injection levels. Typically, it varies from 1 to 2 and can be higher in some cases depending on the diode fabrication process and semiconductor material used.

By assuming that the alphavoltaic battery under irradiation operates as a photovoltaic cell, the device total current density J_{total} that circulates in the external circuit is [23]

$$J_{total} = J_{rad} - J_D - J_{sh},\qquad (4)$$

where J_{rad} is the overall contribution to the current by the carriers generated by alpha particles in three device regions: the DR (J_{DR}), the quasi-neutral emitter regions (J_E) and the base (J_B). The current components J_{DR}, J_E, and J_B have the following forms:

$$J_{DR} = \frac{N_\alpha q E_k (1-R_1)}{\varepsilon_{\mathrm{InGaP}}}\left(e^{-\alpha_{\mathrm{InGaP}} y_1} - e^{-\alpha_{\mathrm{InGaP}} y_2}\right) + \frac{N_\alpha q E_k (1-R_2)}{\varepsilon_{\mathrm{GaAs}}}\left(e^{-\alpha_{\mathrm{InGaP}} y_2} - e^{-\alpha_{\mathrm{InGaP}} y_2 - \alpha_{\mathrm{GaAs}}(y_3 - y_2)}\right),\qquad (5)$$

$$J_E = \left[\frac{N_\alpha q E_k (1-R_0) \alpha_{\text{InGaP}} L_p}{\varepsilon_{\text{InGaP}} (\alpha_{\text{InGaP}}^2 L_p^2 - 1)} \right] \times$$

$$\times \left[\frac{\left(\frac{S_p L_p}{D_p} + \alpha_{\text{InGaP}} L_p \right)}{\left(\frac{S_p L_p}{D_p} \sinh \frac{y_1}{L_p} + \cosh \frac{y_1}{L_p} \right)} - \frac{e^{-\alpha_{\text{InGaP}} y_1} \left(\frac{S_p L_p}{D_p} \cosh \frac{y_1}{L_p} + \sinh \frac{y_1}{L_p} \right)}{\left(\frac{S_p L_p}{D_p} \sinh \frac{y_1}{L_p} + \cosh \frac{y_1}{L_p} \right)} - \alpha_{\text{InGaP}} L_p e^{-\alpha_{\text{InGaP}} y_1} \right] \quad (6)$$

$$J_B = \left[\frac{N_\alpha q E_k (1-R_3) \alpha_{\text{GaAs}} L_n}{\varepsilon_{\text{GaAs}} (\alpha_{\text{GaAs}}^2 L_n^2 - 1)} e^{-\alpha_{\text{GaAs}} (y_4 - y_3)} \right] \times$$

$$\times \left[\alpha_{\text{GaAs}} L_n - \frac{\frac{S_n L_n}{D_n} \left[\cosh \frac{y_4 - y_3}{L_n} - e^{-\alpha_{\text{GaAs}} (y_4 - y_3)} \right]}{\left(\frac{S_n L_n}{D_n} \sinh \frac{y_4 - y_3}{L_n} + \cosh \frac{y_4 - y_3}{L_n} \right)} + \frac{\sinh \frac{y_4 - y_3}{L_n} + \alpha_{\text{GaAs}} L_n e^{-\alpha_{\text{GaAs}} (y_4 - y_3)}}{\left(\frac{S_n L_n}{D_n} \sinh \frac{y_4 - y_3}{L_n} + \cosh \frac{y_4 - y_3}{L_n} \right)} \right] \quad (7)$$

where y_2 is the $In_{0.49}Ga_{0.51}P$ layer thickness, y_3 is the distance between the $In_{0.49}Ga_{0.51}P$ layer surface and the DR edge in the GaAs substrate, N_α is the flux of incident alpha particles, α_{InGaP} and α_{GaAs} are the absorption coefficients of alpha particles, E_k is the kinetic energy of alpha particles, and $S_{n,p}$, $D_{n,p}$, and $L_{n,p}$ are the surface recombination velocities, diffusion constants and diffusion lengths of minority carriers, respectively. The concentrations of donor and acceptor dopants are designated as N_d and N_a, respectively. R_0, R_1, R_2, and R_3 are the reflection coefficients at the cell front surface, the DR edge in the $In_{0.49}Ga_{0.51}P$ layer, the boundary between the $In_{0.49}Ga_{0.51}P$ and GaAs layers, and the DR edge in the GaAs layer, respectively. The average energy required to generate one electron-hole pair by ionization when alpha particles pass through the $In_{0.49}Ga_{0.51}P$ and GaAs regions (*i.e.*, $\varepsilon_{\text{InGaP}}$ and $\varepsilon_{\text{GaAs}}$) is calculated by the following empirical formula [1]:

$$\varepsilon_i(\text{eV}) = 2.67 \times E_{g,i} + 0.87 , \quad (8)$$

where $E_{g,i}$ is the bandgap energy of the respective material ($In_{0.49}Ga_{0.51}P$ or GaAs).

Referring to Eq. (4), the current density through the shunt resistance (J_{sh}) is given by

$$J_{sh} = \frac{V + R_s J_{total}}{R_{sh}} . \quad (9)$$

Finally, the current density across the diode (J_D) under an external bias (V) is given by

$$J_D = J_0 \left[e^{\frac{q(V + R_s J_{total})}{nkT}} - 1 \right] . \quad (10)$$

where J_0 is the reverse saturation current given as

$$J_0 = \frac{q D_p n_{i,\text{InGaP}}^2}{L_p N_d} \times \frac{\frac{S_p L_p}{D_p} \cosh\left(\frac{y_1}{L_p}\right) + \sinh\left(\frac{y_1}{L_p}\right)}{\frac{S_p L_p}{D_p} \sinh\left(\frac{y_1}{L_p}\right) + \cosh\left(\frac{y_1}{L_p}\right)} + \frac{q D_n n_{i,\text{GaAs}}^2}{L_n N_a} \times \frac{\frac{S_n L_n}{D_n} \cosh\left(\frac{y_4}{L_n}\right) + \sinh\left(\frac{y_4}{L_n}\right)}{\frac{S_n L_n}{D_n} \sinh\left(\frac{y_4}{L_n}\right) + \cosh\left(\frac{y_4}{L_n}\right)} . \quad (11)$$

Here, y_1 is the thickness of the neutral region in the $In_{0.49}Ga_{0.51}P$ layer, y_4 is the overall cell thickness (16 µm), k is the Boltzmann constant, T is the temperature, and q is the elementary charge, respectively. The intrinsic carrier concentration has been calculated by the following expression:

$$n_i = \sqrt{N_c N_v} \, e^{-\frac{E_g}{2kT}} , \quad (12)$$

where N_c and N_v are the effective densities in the conduction and valence bands, respectively.

The dependence of the $In_{1-x}Ga_xP$ bandgap energy on the gallium (Ga) stoichiometry is assumed to be [29]

$$E_g(x) = -0.2722 x^2 + 1.1925 x + 1.3399 , \quad (13)$$

while the temperature dependence of the GaAs bandgap energy is expressed as [30]

$$E_g(T) = 1.519 - \frac{\alpha T^2}{\beta + T} \quad (14)$$

with $\alpha = 5.405 \cdot 10^{-4}$ eV/K and $\beta = 204$ K.

The bandgap narrowing effect, which appears when highly doped regions in the device structure are involved, is modeled for the InGaP and GaAs layers by performing the calculations by the following expression:

$$\Delta E_g = A \left(\frac{N}{10^{18}} \right)^{1/3} + B \left(\frac{N}{10^{18}} \right)^{1/4} + C \left(\frac{N}{10^{18}} \right)^{1/2} , \quad (15)$$

where A, B, and C are specific constants as listed in Table 3 [31], and N is the local (total) dopant concentration. This phenomenon is attributed experimentally to the emergence of an impurity band formed by overlapped impurity states.

Table 3. Values of the specific constants (in meV) for calculating the bandgap narrowing effect.

	InGaP (*n*-type)	GaAs (*p*-type)
A	18	9.71
B	9.04	12.19
C	93.46	3.88

To describe the dependence of the carrier mobility in the $In_{0.49}Ga_{0.51}P$ and GaAs layers on the doping level, a low field mobility model based on the Caughey and Thomas expression at room temperature [32] is used:

$$\mu_{n,p} = \mu_{0n,p}^{\min} + \frac{\mu_{0n,p}^{\max} - \mu_{0n,p}^{\min}}{1 + \left(\frac{N}{N_{n,p}^{crit}}\right)^{\delta_{n,p}}}. \quad (16)$$

The model reference parameters $\mu_{0n,p}^{\min}$, $\mu_{0n,p}^{\max}$, $N_{n,p}^{crit}$, and $\delta_{n,p}$ are listed in Table 4.

After calculating $J(V)$ characteristics, the conversion efficiency (or alphavoltaic efficiency) η is defined as the ratio of the maximum output electric power $P_{\max}$ generated by the heterojunction battery to the power density of the incident alpha particles:

$$\eta = \frac{P_{\max}}{P_{inc}} = \frac{J_{MPP} \times V_{MPP}}{P_{inc}}, \quad (17)$$

where P_{inc} is given by [8]

$$P_{inc} = 3.7 \cdot 10^{10} \cdot qAZE_{av}. \quad (18)$$

Here, A, Z and E_{av} are the apparent activity density, the decay mode coefficient, and the average energy of alpha particles emitted by the Am^{241} source. For alpha decay, Z takes the value of 2 [16].

Charge accumulation at the two battery electrodes creates an open-circuit voltage V_{oc} across the battery terminals expressed as

$$V_{oc} = \frac{nkT}{q} \times \ln\left(\frac{J_{sc}}{J_0} + 1\right). \quad (19)$$

Table 4. Reference parameters for the Caughey and Thomas carrier mobility model at $T = 300$ K.

	$In_{0.49}Ga_{0.51}P$	GaAs
$\mu_{0n,p}^{\min}$ (cm^2/V·s)	400, 15	0
$\mu_{0n,p}^{\max}$ (cm^2/V·s)	4300, 150	9400, 400
$N_{n,p}^{crit}$ (cm^{-3})	$2 \cdot 10^{16}$, $1.5 \cdot 10^{17}$	$1 \cdot 10^{17}$, $1.6 \cdot 10^{18}$
$\delta_{n,p}$	0.7, 0.8	0.5, 1

Table 5. Simulation parameters at $T = 300$ K.

R_0	R_1	τ_h(s)	S_p (cm/s)	S_n (cm/s)
0.05	0.1	10^{-8}	10^5	10^5
R_2	R_3	τ_e(s)	n	S(cm^2)
0.15	0.2	$2 \cdot 10^{-8}$	1.55	1

At zero voltage ($V = 0$), the short-circuit current density is exactly J_{rad}.

The fill-factor (FF) of the battery is defined by the ratio

$$FF = \frac{P_{\max}}{J_{sc} V_{oc}}. \quad (20)$$

4. Results and discussion

4.1. Doping influence

The heterojunction depth is 0.2 μm. During the simulations, the doping level of the emitter (*n*-type) was varied from $1 \cdot 10^{17}$ to $5 \cdot 10^{19}$ cm^{-3}, while the doping level of the base (*p*-type) was varied from $1 \cdot 10^{16}$ (intrinsic carrier concentration) to $5 \cdot 10^{18}$ cm^{-3}. The other fundamental physical parameters of the device are summarized in Table 5.

The influence of the dopant concentrations on the battery performance is shown in Fig. 2.

The main figures of merit (FOMs) of the device, namely η, P_{max}, J_{sc}, V_{oc}, and FF, are calculated for a default radioactivity density of 0.2 mCi/cm^2 and an alpha-particle average energy of 5.485 MeV.

We can see that for donor and acceptor concentrations of $3 \cdot 10^{19}$ and $5 \cdot 10^{16}$ cm^{-3}, respectively, the battery conversion efficiency exhibits a maximum value of 7.05%, while $P_{\max}$, J_{sc}, V_{oc}, and FF are equal to 0.91 μW/cm^2, 1.17 μA/cm^2, 1.06 V, and 73.94%, respectively. More specifically, both the maximum electric power and the conversion efficiency start to increase with the doping level up to the mentioned dopant concentrations. After this, the battery performance gradually decreases. This result may be explained by analyzing the behavior of V_{oc} and J_{sc}. In fact, increase of the doping level (especially in the base layer) leads to enhancement of V_{oc} and J_{sc} and, hence, the conversion efficiency. In accordance with Eq. (11), an inverse dependence of the reverse saturation current J_0 on the dopant concentration should be taken into account. Therefore, the open-circuit voltage V_{oc} increases with the decrease of J_0 (Eq. (19)). Furthermore, the bandgap narrowing effect tends to enhance generation of free carriers in the device structure. However, higher doping levels ($N_d > 3 \cdot 10^{19}$ cm^{-3} and $N_a > 5 \cdot 10^{16}$ cm^{-3}) reduce both the diffusion lengths and the mobilities of minority carriers thus decreasing J_{sc} and the conversion efficiency as shown in Fig. 2.

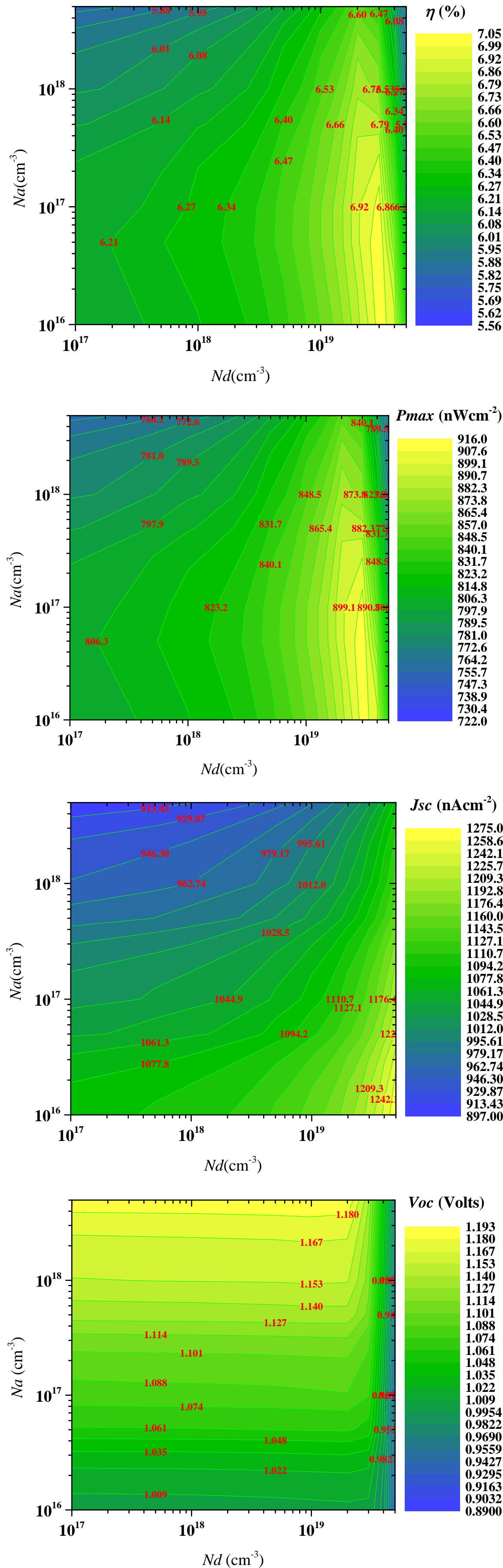

Fig. 2. Variation of η, $P_{\max}$, J_{sc}, V_{oc}, and FF with N_a and N_d.

4.2. Effect of surface recombination velocity

From the literature, various numerical and experimental studies have been focused on the effects of surface recombination velocity (SRV) in semiconductor devices [33, 34]. In fact, surface recombination phenomena, which are non-radiative recombination processes, mainly occur due to defects and impurities (*e.g.*, recombination centers) contained within the semiconductor crystal lattice. These processes may be dominant in determining the device effective current capabilities [33]. With this in mind, we have evaluated the SRV impact on the battery performance by using several simulations. As expected, the overall performance of the proposed InGaP/GaAs alphavoltaic battery is highly influenced by the SRV value and, in fact, the key parameters V_{oc}, J_{sc}, $P_{\max}$, and η decrease at high SRVs. In particular, to investigate the SRV effects, we have considered the values of the front surface recombination velocity (FSRV), S_p, and the back surface recombination velocity (BSRV), S_n, in the ranges of $5\cdot10^2\ldots10^6$ and $5\cdot10^3\ldots10^6$ cm/s, respectively.

The impact of the FSRV and BSRV values on the device FOMs obtained by calculating the $J(V)$ and $P(V)$ characteristics of the battery is shown in Figs. 3 and 4.

As can be seen from Fig. 3, η and $P_{\max}$ decrease sharply when the recombination velocity on both the front and the back surface increases. More specifically, for FSRV = BSRV = 10^6 cm/s, η and $P_{\max}$ are equal to 5.84% and 0.76 μW/cm^2, respectively. These values steeply increase to 8.25% and 1.07 μW/cm^2, respectively, when FSRV decreases to $5\cdot10^2$ cm/s and BSRV decreases to $5\cdot10^3$ cm/s, indicating the enhanced recombination losses at higher SRVs. At the same time, as depicted in Fig. 4 and expected from Eqs. (3)–(5), (9), and (17), J_{sc} and V_{oc} increase with the decrease of the FSRV and BSRV values.

In particular, when FSRV and BSRV decrease from 10^6 cm/s to $5\cdot10^2$ and $5\cdot10^3$ cm/s, respectively, J_{sc} and V_{oc} increase from 1.02 μA/cm^2 and 0.98 V to 1.31 μA/cm^2 and 1.11 V, respectively. Analyzing the influence of FSRV and BSRV on FF, we find that FF peaks to 77.41% at FSRV = $5\cdot10^2$ cm/s and BSRV = 10^6 cm/s and gradually decreases to 73.67% at FSRV = 10^6 cm/s and BSRV = 10^5 cm/s.

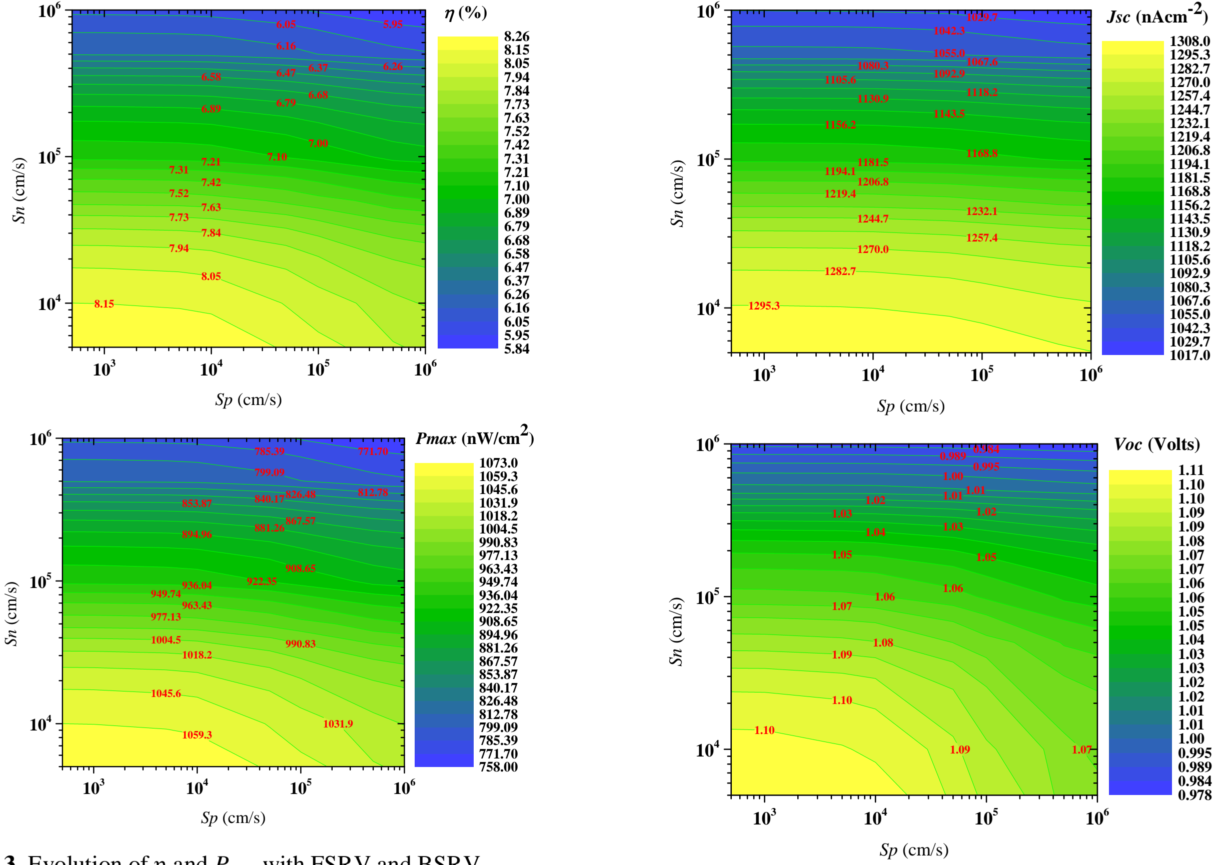

Fig. 3. Evolution of η and P_{max} with FSRV and BSRV.

It may be concluded that the SRV parameters have an important influence on the device performance. Therefore, it is critical to reduce the SRV at both the front and back surfaces. For example, in designing high performance alphavoltaic batteries, it could be useful to reduce the number of dangling bonds at the surface by depositing a passivation layer.

4.3. Impact of Am^{241} apparent activity density

Am^{241} radioisotope is an effective power supply for the proposed alphavoltaic battery. In general, physical properties of a radioisotope, such as the type of radiation emitted, the radioactivity intensity, the decay energy, and the half-life, all affect the performance of a nuclear battery. Therefore, it is very important to evaluate the radioisotope properties that fit the required battery design criteria.

In this study, we considered a unidirectional alpha-radiation Am^{241} source with an apparent activity density $A = 0.2$ mCi/cm^2. The source was placed at the optimum distance to the junction that corresponds to the maximum energy delivered by the alpha particles inside the device. In this section, we investigate the impact of the apparent activity density of the Am^{241} radioisotope in the range of 0.2 to 2.4 mCi/cm^2 on the electrical characteristics of the proposed heterojunction. For simulating the $J(V)$ and $P(V)$ characteristics, the other device parameters were fixed to the values $N_d = 3\cdot10^{19}$ cm^{-3}, $N_a = 5\cdot10^{16}$ cm^{-3}, $S_p = 5\cdot10^2$ cm/s, $S_n = 5\cdot10^3$ cm/s, and $y_1 = 0.2$ µm.

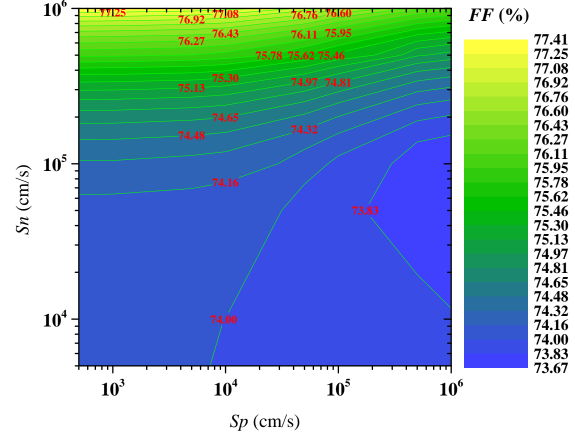

Fig. 4. Evolution of J_{sc}, V_{oc} and FF with FSRV and BSRV.

Fig. 5 shows that both the conversion efficiency and the electric output power density of the battery remarkably increase with the increase of the Am^{241} apparent activity density. Moreover, J_{sc} and V_{oc} as functions of A show similar behavior (see Fig. 6). The observed variations are due to the direct proportionality between J_{sc} and the alpha-particles flux that depends on A. More specifically, we achieve the conversion efficiency of 10.31% and the electric power density of 16.07 µW/cm^2 at $A = 2.4$ mCi/cm^2. The other FOMs of the battery improve from J_{sc} = 1.31 µA/cm^2, V_{oc} = 1.11 V, and FF = 84.94% at $A = 0.2$ mCi/cm^2 to J_{sc} = 15.69 µA/cm^2, V_{oc} = 1.21 V, and FF = 85.85% at $A = 2.4$ mCi/cm^2.

It can be seen from Fig. 5 that the conversion efficiency increases to 12.58% and the output power density is 19.62 μW/cm^2 at A = 2.4 mCi/cm^2 when reflection of alpha particles as well as ohmic losses are neglected.

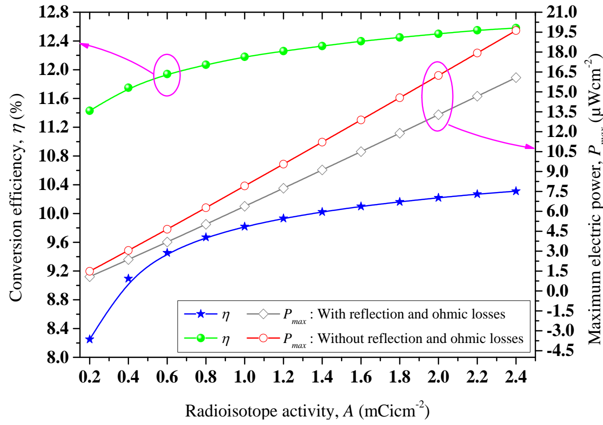

Fig. 5. η and P_{max} *versus A.*

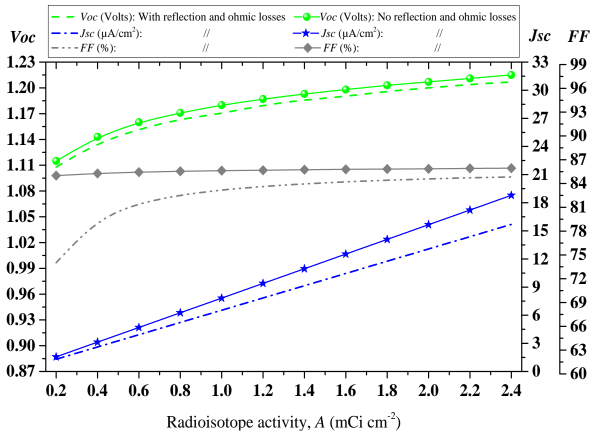

Fig. 6. J_{sc} and V_{oc} *versus A.*

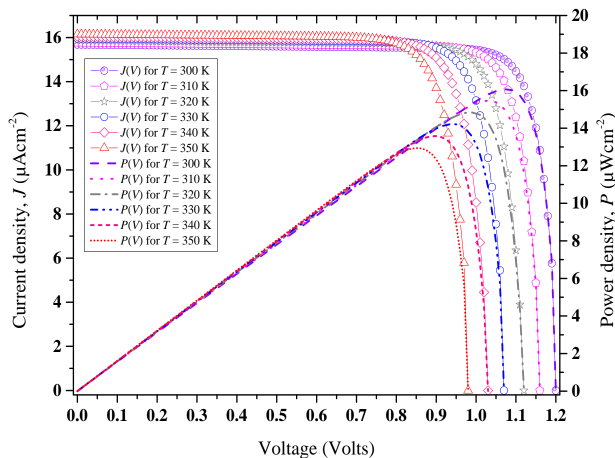

Fig. 7. Variations of $J(V)$ and $P(V)$ characteristics with temperature.

4.4. Impact of temperature

The $J(V)$ characteristics for an apparent activity density of 2.4 mCi/cm^2 shown in Fig. 7 evidence an increase of the short-circuit current and a decrease of the open-circuit voltage when increasing the device operation temperature from 300 to 350 K.

This behavior may be explained by taking into account the temperature dependence of the bandgap energy. In particular, a temperature increase causes a reduction in the material bandgap width, and, therefore, the reverse saturation current in the device structure tends to increase. This variation causes a reduction of the open-circuit voltage, and the mechanism of carriers generation becomes increasingly significant leading to an increase of the short-circuit current as shown in Fig. 8. It may be also seen in Fig. 8 that the fill factor decreases with increasing the value of T, following the increase of the dark saturation current. The decrease in FF is caused by the fact that the decrease of the open circuit voltage is more significant than the increase of the short circuit current. The device conversion efficiency also decreases as shown in Fig. 9.

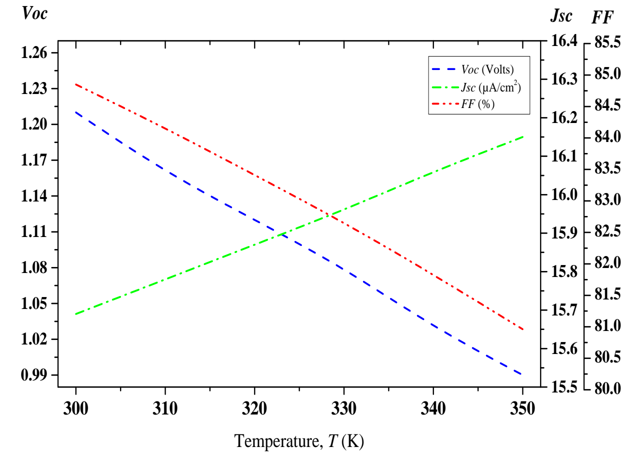

Fig. 8. Variations of J_{sc} ,V_{oc}, and FF with temperature.

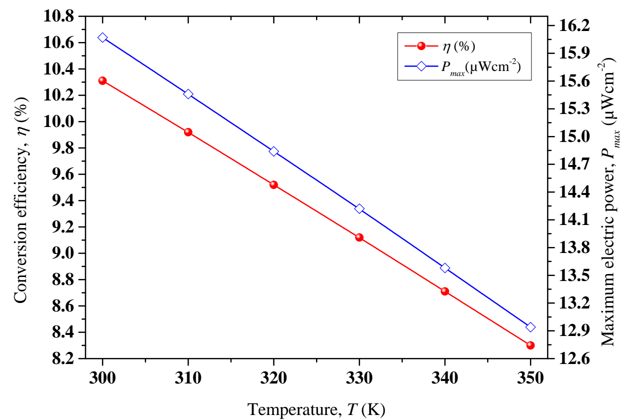

Fig. 9. Variations of η and P_{max} with temperature.

Summarizing, these four parameters η, P_{max}, V_{oc}, and *FF* linearly decrease with the increase of the temperature from 10.31%, 16.07 μW/cm², 1.21 V, and 85.0% at T = 300 K to 8.30%, 12.94 μW/cm², 0.99 V, and 80.96% at T = 350 K, respectively. On the other hand, J_{sc} weakly increases from 15.69 μA/cm² at T = 300 K to 16.15 μA/cm² at T = 350 K.

5. Conclusions

An *n-p* $In_{0.49}Ga_{0.51}P$/GaAs heterojunction battery has been proposed and evaluated as a practical carrier separating structure to convert the energy of alpha particles emitted by an Am^{241} source to electrical power. Theoretical calculations have been made to evaluate the battery performance. It has been found that the proposed device can provide a power density of about 16 μW/cm² being irradiated by an Am^{241} emitter with a decay energy density of 2.4 mCi/cm² at T =300 K. By increasing the temperature to T = 350 K, the maximum output power decreases to about 13 μW/cm².

By optimizing the battery structure and connecting alphavoltaic batteries in series or shunt configurations, the output power density can be increased to the levels required for practical use to power the next-generation electronic systems.

References

1. Prelas M., Boraas M., Aguilar F. *et al*. *Lecture Notes in Energy. Nuclear Batteries and Radioisotopes.* **56**. Springer, Switzerland, 2016. https://doi.org/10.1007/978-3-319-41724-0.
2. Rappaport P. The electron-voltaic effect in *p-n* junctions induced by beta particle bombardment. *Phys. Rev*. 1954. **93**. P. 246–247. https://doi.org/10.1103/PhysRev.93.246.2.
3. Krasnov A., Legotin S., Kuzmina K. *et al*. A nuclear battery based on silicon *p-i-n* structures with electroplating ^{63}Ni layer. *Nucl. Eng. Technol*. 2019. **51**. P. 1978–1982. https://doi.org/10.1016/j.net.2019.06.003.
4. Bouzid F., Pezzimenti F., Dehimi L. Modelling and performance analysis of a GaN-based *n/p* junction betavoltaic cell. *Nucl. Instrum. Methods Phys. Res. A*. 2020. **969**. P. 164103. https://doi.org/10.1016/j.nima.2020.164103.
5. Munson C.E., Gaimard Q., Merghem K. *et al*. Modeling, design, fabrication and experimentation of a GaN-based ^{63}Ni betavoltaic battery. *J. Phys. D: Appl. Phys*. 2018. **51**. P. 035101. http://dx.doi.org/10.1088/1361-6463/aa9e41.
6. Bouzid F., Saeed M.A., Carotenuto R., Pezzimenti F. Design considerations on 4H-SiC-based *p-n* junction betavoltaic cells. *Appl. Phys. A*. 2022. **128**. P. 234. https://doi.org/10.1007/s00339-022-05374-7.
7. Svintsov A.A., Krasnov A.A., Polikarpov M.A. *et al*. Betavoltaic battery performance: comparison of modeling and experiment. *Appl. Radiat. Isot*. 2018. **137**. P. 184–189. https://doi.org/10.1016/j.apradiso.2018.04.010.
8. Bormashov V., Troschiev S., Volkov A. *et al*. Development of nuclear microbattery prototype based on Schottky barrier diamond diodes. *phys. status solidi (a)*. 2015. **212**. P. 2539. https://doi.org/10.1002/pssa.201532214.
9. Liu Y.-M., Lu J.-B., Li X.-Y. *et al*. Theoretical prediction of diamond betavoltaic batteries performance using ^{63}Ni. *Chin. Phys. Lett*. 2018. **35**. P. 072301. https://doi.org/10.1088/0256-307X/35/7/072301.
10. Spencer M.G., Alam T. High power direct energy conversion by nuclear batteries. *Appl. Phys. Rev*. 2019. **6**. P. 031305. https://doi.org/10.1063/1.5123163.
11. Khvostikov V.P., Kalinovskiy V.S., Sorokina S.V. *et al*. Tritium power supply sources based on AlGaAs/GaAs heterostructures. *Techn. Phys. Lett*. 2019. **45**. P. 1197–1199 https://doi.org/10.1134/S1063785019120083.
12. Bouzid F., Dehimi S., Hadjab M. *et al*. Performance prediction of AlGaAs/GaAs betavoltaic cells irradiated by nickel-63 radioisotope. *Physica B: Condensed Matter*. 2021. **607**. P. 412850. https://doi.org/10.1016/j.physb.2021.412850.
13. Cress C.D., Landi B.J., Raffaelle R.P., Wilt D.M. InGaP alpha voltaic batteries: Synthesis, modeling, and radiation tolerance. *J. Appl. Phys*. 2006. **100**. P. 114519. https://doi.org/10.1063/1.2390623.
14. Cress C.D., Landi B.J., Raffaelle R.P. Modeling laterally-contacted nipi-diode radioisotope batteries. *IEEE Trans. Nucl. Sci*. 2008. **55**. P. 1736. https://doi.org/10.1109/lisat.2008.4638957.
15. Bouzid F., Kayahan E., Pezzimenti F. Thorium-228 as emitting source for InGaP/GaAs-based heterojunction alphavoltaic cells. *Appl. Phys. A*. 2023. **129**. P. 554. https://doi.org/10.1007/s00339-023-06829-1.
16. Qiao D.Y., Chen X.J., Ren Y., Yuan W.Z. A micro nuclear battery based on SiC Schottky barrier diode. *J. Microelectromech Syst*. 2011. **20**, No 3. P. 685–690. https://doi.org/10.1109/JMEMS.2011.2127448.
17. Bouzid F., Pezzimenti F., Dehimi L. *et al*. Analytical modeling of dual-junction tandem solar cells based on an InGaP/GaAs heterojunction stacked on a Ge substrate. *J. Electron. Mater*. 2019. **48**. P. 4107–4116. https://doi.org/10.1007/s11664-019-07180-z.
18. Duan W., Lambertz A., Bittkau K. *et al*. A route towards high-efficiency silicon heterojunction solar cell. *Prog. Photovolt. Res. Appl*. 2022. **30**. P. 384. https://doi.org/10.1002/pip.3493.
19. Langley J., Litz M., Russo J., Ray W. Jr. Design of Alpha-Voltaic Power Source Using Americium-241 (^{241}Am) and Diamond with a Power Density of 10 mW/cm³. *Technical Report*, ARL-TR-8189, OCT 2017. US Army Research Laboratory.
20. Xu J., Guo M., Lu M. *et al*. Effect of alpha-particle irradiation on InGaP/GaAs/Ge triple-junction solar cells. *Materials*. 2018. **11**. P. 944. https://doi.org/10.3390/ma11060944.
21. Okuno Y., Okuda S., Oka T. *et al*. Performance degradation of InGaP solar cells due to 70 keV electron irradiation. *Jpn. J. Appl. Phys*. 2017. **56**. P. 081203. https://doi.org/10.7567/JJAP.56.081203.

22. Kınacı B., Özen Y., Kızılkaya K. *et al.* Study on growth and characterizations of $Ga_xIn_{1-x}P$/GaAs solar cell structure. *J. Mater. Sci.: Mater. Electron.* 2013. **24**. P. 3269. https://doi.org/10.1007/s10854-013-1242-y.
23. Sze S.M. and Ng K.K. *Physics of Semiconductor Devices*, Third Ed. John Wiley, Interscience, 2006.
24. https://www.ioffe.ru/SVA/NSM/Semicond/GaAs/basic.html (last accessed on: 05/02/2024).
25. https://www.ioffe.ru/SVA/NSM/Semicond/GaInP/basic.html (last accessed on: 05/02/2024).
26. Keith S., Doyle J.R., Harper C. *et al*. Toxicological Profile for Radon, Atlanta (GA): Agency for Toxic Substances and Disease Registry (US); 2012 May.
27. Magill J., Pfennig G., Galy J. *European Commission Joint Research Centre Institute for Transuranium Elements*, 2006.
28. Bower K.E., Barbanel Y.A., Shreter Y.G., Bohnert G.W. *Polymers, Phosphors, and Voltaics for Radioisotope Microbatteries*, First ed., CRC Press, New York, 2002.
29. Haas A.W., Wilcox J.R., Gray J.L., Schwartz R.J. Design of a GaInP/GaAs tandem solar cell for maximum daily, monthly, and yearly energy output. *J. Photon. Energy*. 2011. **1**. P. 018001. https://doi.org/10.1117/1.3633244.
30. Levinshtein M.E., Rumyantsev S.L., Shur M. *Handbook Series on Semiconductor Parameters*. **1**. World Scientific, London, 1996. P. 77–103.
31. Jain S.C., Roulston D.J. A simple expression for band gap narrowing (BGN) in heavily doped Si, Ge, GaAs and Ge_xSi_{1-x} strained layers. *Solid-State Electron*. 1991. **34**. P. 453. https://doi.org/10.1016/0038-1101(91)90149-S.
32. Caughey D.M., Thomas R.E. Carrier mobilities in silicon empirically related to doping and field. *Proc. IEEE*. 1967. **55**. P. 2192. https://doi.org/10.1109/proc.1967.6123.
33. Da Y., Xuan Y. Role of surface recombination in affecting the efficiency of nanostructured thin-film solar cells. *Opt. Express*. 2013. **21**. P. 1065. https://doi.org/10.1364/OE.21.0A1065.
34. Ali K., Khan H.M., Anmol M. *et al*. Effect of surface recombination velocity (SRV) on the efficiency of silicon solar cell. *J. Optoelectron. Adv. Mater.* 2020. **22**, Issue 5–6. P. 251–255.

Authors' contributions

Bouzid F.: conceptualization, methodology, formal analysis, investigation, data curation, writing – original draft, writing – review & editing, visualization.
Kayahan E.: investigation, writing – review & editing.
Saeed M.A.: investigation, writing – review & editing.
Babes B.: investigation, writing – review & editing.
Ghoneim S.S.M.: investigation, writing – review & editing.
Pezzimenti F.: investigation, writing – review & editing.

Authors and CV

Fayçal Bouzid received his PhD degree in Materials Physics from the University of Biskra, Algeria, in 2018. He is a Senior Researcher at the Research Center in Industrial Technologies CRTI-Algeria. The area of his scientific interests includes physics and technology of semiconductor materials, hetero- and hybrid structures and devices (solar cells, thermo-photovoltaics, nuclear micro-batteries, UV and IR photodetectors, and laser sources).
https://orcid.org/0000-0002-2237-4789

Ersin Kayahan received his PhD degree from the Kocaeli University, Turkey, in 2003. His current fields of interest include lasers, laser materials interactions, nanoparticles, optical roughness, optical sensors, porous silicon, luminescence, laser ablation, and surface processing. He is also an expert in nanoparticles produced by laser ablation. Nowadays he carries on research on medical applications of lasers. E-mail: kayahan@kocaeli.edu.tr,
https://orcid.org/0000-0001-8657-2947

Mohammad Alam Saeed received his M.Sc. degree from the University of Punjab, Lahore, Pakistan, and the Ph.D. degree from the University at Albany, NY, USA, and the Stanford Linear Accelerator Center, CA, USA, in 1997 and 2009, respectively. From 2002 to 2004, he was in the Albany High Energy Physics Group, State University of New York, Albany. He was a Senior Lecturer at the University Technology Malaysia. At present he works at the University of Education, Lahore, Pakistan. His research interests are radiation, health physics, and computational materials science. E-mail: alam.saeed@ue.edu.pk,
http://orcid.org/0000-0002-3529-9255

Badreddine Babes received his M.S. and Ph.D. degrees in Electrical Engineering from the University of Setif-1, Algeria, in 2010 and 2018, respectively. Since 2017, he works at the Research Center in Industrial Technologies CRTI-Algeria. His current research interests include predictive control of linear and nonlinear systems applied in motor drives and renewable energy systems, and pulse current control of gas metal arc welding processes. E-mail: b.babes@crti.dz,
https://orcid.org/0000-0002-9256-2021

Sherif S. M. Ghoneim received his M.Sc. degree from the Faculty of Engineering at Shoubra, Zagazig University, Egypt, in 2000. He received his Ph.D. degree in Electrical Power and Machines from the Faculty of Engineering, Cairo University, in 2008. Since 1996, he has been teaching at the Faculty of Industrial Education, Suez Canal University, Egypt. From 2005 to 2007, he was a Guest Researcher at the Institute of Energy Transport and Storage (ETS), University of Duisburg–Essen, Germany. He is currently an Associate Professor at the Electrical Engineering Department, Faculty of Engineering, Taif University.
E-mail: s.ghoneim@tu.edu.sa,
https://orcid.org/0000-0002-9387-1950

Fortunato Pezzimenti received his Laurea and Ph.D. degrees in Electronic Engineering from the Mediterranea University of Reggio Calabria, Italy, in 2000 and 2004, respectively. Since 2006, he is an Assistant Professor of Electronics at the Mediterranea University of Reggio Calabria. His current research interests include design, modeling, and electrical characterization of wide bandgap semiconductor devices for high-power, high-frequency, and high-temperature applications.
E-mail: fortunato.pezzimenti@unirc.it,
https://orcid.org/0000-0002-8410-0142

Моделювання високопотужної альфа-вольтаїчної батареї на основі гетеропереходу InGaP/GaAs, опромінюваного випромінюванням америцію-241

F. Bouzid, E. Kayahan, M.A. Saeed, B. Babes, S.S.M. Ghoneim, F. Pezzimenti

Анотація. Конструкцію структур на основі напівпровідникових гетеропереходів можна покращити для підвищення ефективності ядерних мікробатарей. У цій роботі з використанням лабораторного програмного забезпечення досліджено альфа-вольтаїчну батарею малої потужності. Ядерна батарея складається з гетероструктури $In_{0,49}Ga_{0,51}P/GaAs$, опромінюваної альфа-частинками америцію-241 (Am^{241}) з середньою кінетичною енергією 5.485 МеВ. Загальна активна площа альфа-вольтаїчної батареї становить 1 см^2. З використанням комплексної аналітичної моделі промодельовано залежності густини струму $J(V)$ і вихідної електричної потужності $P(V)$ від напруги та визначено величину ефективності перетворення енергії. Модель враховує відбиття падаючих альфа-частинок, омічні втрати, ефект межі між двома шарами та границь області виснаження. З метою оптимізації продуктивності батареї моделювання проводили при різних значеннях ефективної густини активності радіоізотопу, концентрацій легуючої домішки в емітері та базі, а також швидкості поверхневої рекомбінації як у фронтальному, так і тильному шарах. Результати дослідження показують, що при опроміненні з джерела Am^{241} з потужністю 2.4 мКі/см^2 ефективність перетворення енергії батареї може досягати 10.31% при максимальному значенні густини вихідної потужності у 16.07 мкВт/см^2. Отже, гетероструктура $In_{0,49}Ga_{0,51}P/GaAs$ у поєднанні з Am^{241} є багатообіцяючою конструкцією для забезпечення довгострокового енергопостачання в суворих умовах.

Ключові слова: альфа-вольтаїчна батарея, гетероструктура, америцій-241, альфа-частинки, омічні втрати.